THE JOURNAL OF PHYSICAL CHEMISTRY B

Article

pubs.acs.org/JPCB

High-Resolution Single-Molecule Recognition Imaging of the Molecular Details of Ricin–Aptamer Interaction

Bin Wang,[†] Cunlan Guo,[†] Mengmeng Zhang,[†] Bosoon Park,[‡] and Bingqian Xu*[,†]

[†]Single Molecule Study Laboratory, Faculty of Engineering and Nanoscale Science and Engineering Center, University of Georgia, Athens, Georgia 30602, United States

[‡]USDA-ARS, Russell Research Center, Athens, Georgia 30605, United States

Supporting Information

ABSTRACT: We studied the molecular details of DNA aptamer–ricin interactions. The toxic protein ricin molecules were immobilized on a Au(111) surface using a *N*-hydroxysuccinimide (NHS) ester to specifically react with lysine residues located on the ricin B chains. A single ricin molecule was visualized in situ using the AFM tip modified with an antiricin aptamer. Computer simulation was used to illustrate the protein and aptamer structures, the single-molecule ricin images on a Au(111) surface, and the binding conformations of ricin–aptamer and ricin–antibody complexes. The various ricin conformations on a Au(111) surface were caused by the different lysine residues reacting with the NHS ester. It was also observed that most of the binding sites for aptamer and antibody on the A chains of ricin molecules were not interfered by the immobilization reaction. The different locations of the ricin binding sites to aptamer and antibody were also distinguished by AFM recognition images and interpreted by simulations.

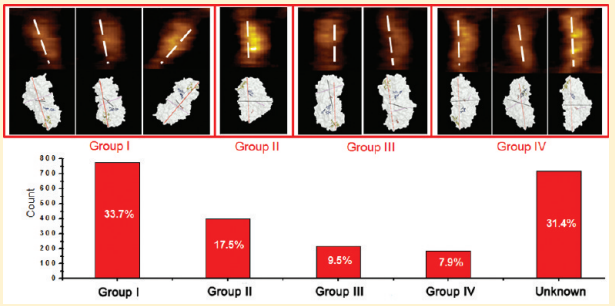

INTRODUCTION

Protein–nucleic acid interactions play important roles in the physiological behavior of living cells and therefore have drawn increasing attention in recent years.[1,2] The structure–function relationships of biomolecules (such as proteins, DNAs, and RNAs) are the keys to understanding their properties and interactions. For example, ricin is one of the most potent naturally occurring toxic proteins, and 500 μg of ricin can kill an adult.[3] According to the study on ricin toxicology, ricin A chain acts as a glycosidase that removes one adenine residue from the loop of the 28S rRNA, causing this rRNA to lose its function during protein synthesis.[4] Therefore, the study of the interactions between ricin protein and other biospecies has a potential impact on both fundamental research and biomedicine applications. Various techniques have been used to investigate the function of the ricin molecule and its interactions with antibody or nucleic acids. Mutagenesis and X-ray crystallography were widely used to study the active residues of the ricin A chain to the ribosome.[5] Small ring molecules were also used to study the mechanism of ricin toxicology.[6] Some other techniques, including competition assay,[7] electrophoresis,[8] antibody array,[9] surface plasmon resonance (SPR),[10] surface-enhanced Raman scattering (SERS),[11] nanopore,[12] nanoparticle,[13] molecular imprinting,[14] and atomic force microscopy (AFM),[15,16] have also been used for study of ricin toxicology or ricin detection. Most of the previous studies relied on spectroscopic or electrochemical methods to investigate the physical and chemical properties of ricin, while AFM is a technique that is capable of providing high-resolution single-molecule images of proteins and nucleic acids in aqueous solution. Therefore, AFM is widely used in biological science to study the biophysical properties of different biospecies.[17] For most protein–nucleic acid complexes, conventional experimental methods, such as X-ray crystallography and nuclear magnetic resonance (NMR), require numerous efforts and hign cost to obtain their detailed structural information. However, AFM images can provide detailed information for this type of biomolecular interaction with relatively low cost and minute sample consumption. Although AFM single-molecule recognition techniques have been used on studies of protein–ligand and protein–protein interactions, detailed information on the molecular structures and interactions is still in great need and deserves more careful investigation.[15,18,19]

Recently, aptamer has been used to successfully study ricin–nucleic acid interactions.[7,8,19−22] Aptamers are versatile binding reagents that show interactions with a wide range of targets such as small molecules, lipids, proteins, carbohydrates, viruses, and cells.[23] Some aptamer research has even led to medical applications and FDA-approved clinical trials.[23,24] DNA aptamers have a relatively lower cost and are more stable than antibody. Therefore, biosensing and molecular recognition using DNA aptamers have become an emerging research area. In particular, for the study of interactions between proteins and

Received: February 22, 2012
Revised: April 8, 2012
Published: April 10, 2012

nucleic acids, aptamers can be used as analog models and probes.

In order to keep the biospecies active and mimic the physiological conditions of their interactions, the probe molecule in AFM experiments needs to be attached on the tip surface by a string of linker molecules, mostly heterobifunctional polyethylene glycol molecules. The target molecule is immobilized on sample substrate, such as Au (111) coated on mica, with the help of cross-linker molecules.[25,26] Surface immobilization methods play an important role in this type of study because the chemical reactions used to immobilize the target molecules determine their conformations on the substrate and in turn influence the interactions between probe and target molecules.

Here we use the DNA aptamer with specific affinity to ricin as a probe to study the ricin−nucleic acids interactions. The linker molecule, the lipoic acid-*N*-hydroxysuccinimide (LA-NHS) ester, was used to bond covalently with the lysine residues on the ricin surface.[16,27] We then immobilized ricin molecules on a Au(111) surface and tested the activities of their binding sites to aptamer.[16] AFM molecular recognition experiments were conducted to compare the recognition signals generated by antiricin aptamer and antiricin antibody, respectively. The results are shown in the Results and Discussion. When the ricin molecule is immobilized on a Au(111) surface with the lysine−NHS reaction, reactions of the nine different lysine residues on the ricin surface are supposed to determine which side of the ricin molecule will be contacting the substrate and which side will be exposed to bulk solution (Figure 1). We used this NHS ester reaction to control the

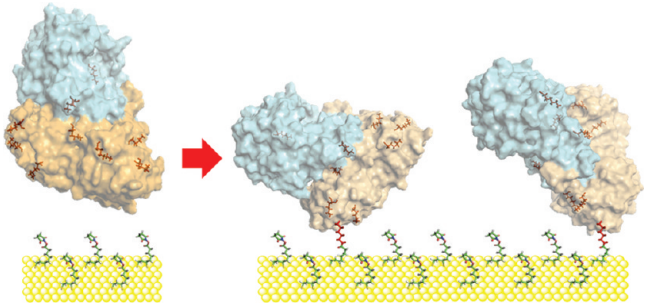

Figure 1. Schematics of ricin immobilization on Au(111) surface. Nine lysine residues are colored in red, including ricin A chain K4, K239, B chain K40, K52, K62, K168, K203, K219, and K243.

conformations and orientations of the ricin molecule on the gold substrate, and high-resolution AFM images showed the detailed morphologies of these ricin molecules reacting with different lysine residues. Analysis of these nine conformations with AFM topography images are shown later in the Results and Discussion.

Compared to the high-resolution structural information obtained by X-ray crystallography and NMR, current AFM techniques have difficulty in showing atomic details for biomolecules due to the resolution limits. Therefore, AFM experimental data need help from biological theory and computer simulations to explain the observed phenomenon. On the other hand, simulations also need experimental data to improve their models so that the simulation results will have a more meaningful impact on the real world. Recently, computational simulations were increasingly used to study aptamers and their interactions with other molecules.[28−30] Here, we used computer simulations to verify the phenomenon and proposed mechanisms of our AFM recognition experiments. The binding sites on ricin and aptamer were predicted by molecular modeling and tested by blocking experiments. The molecular modeling methods used in this study include molecular dynamics and molecular docking. They provide helpful guides to study structure−function relationship of aptamer binding because structural information on the aptamer and its binding conformation with ricin are not available. In particular, the docking and prediction of binding sites helped explain the AFM molecular recognition signal and the different ricin conformations observed on the Au(111) surface.

MATERIALS AND METHODS

The aptamer sequence was obtained from the literature and purchased from Integrated DNA Technologies (Coralville, IA, USA), and the 5′ terminal was modified with a short hydrocarbon linker and amine group.[8] The ricin sample molecule was purchased from Vector Laboratories (Burlingame, CA). The linker molecule HS-PEG-COOH (MW 2000) was purchased from Creative PEGWorks (Winston Salem, NC, USA). *N*-Hydroxysuccinimide (NHS) was purchased from Sigma-Aldrich (St. Louis, MO, USA). 1-(3-Dimethylaminopropyl)-3-ethylcarbodimide hydrochloride (EDC) was purchased from Flucka Chemicals (Sigma-Aldrich, St. Louis, MO, USA). LA-NHS was synthesized in our lab. Phosphate buffer saline (PBS, pH 7.2) was purchased from Pierce (Thermo Scientific, Waltham, MA, USA). Triple DI water was further purified by a Barnstead Nanopure Diamond Laboratory Water System (18 MΩ).

The gold-coated AFM tip was chemically modified with HS-PEG-COOH via the Au−S bond. Consequently, the amine-modified aptamer was attached to the carboxyl group of the PEG molecule with the help of NHS/EDC solution. Reactions involved in this process are shown in Figure 2. Reaction details are listed in SI-1, Supporting Information. The PEG polymer was used here to provide enough freedom for the attached aptamer molecule so that the possible binding sites of the aptamer will not be interfered during the scanning.[31] Ricin molecules were immobilized on the Au(111) surface by reaction between lysine residues on the ricin surface and LA-NHS molecules on the gold surface. Reactions involved in this process were reported in a previous publication.[16,32]

AFM imaging was conducted in TopMAC mode with the additional module of PicoTREC (Agilent Technologies, Santa Clara, CA) to obtain the topography images of ricin in PBS pH 7.2 buffer solution. In addition, the interaction between aptamer and ricin during AFM scanning generates recognition signals and is shown in the recognition images.

To test the interaction/binding specificity of the aptamer with ricin, blocking experiments were also conducted. The 1.0 μM aptamer solution in PBS pH 7.2 (blocking solution) was injected into the flow-through liquid cell during AFM imaging, and scanning was focused in the fixed area. Therefore, the images on the same scan area before and after injection of blocking solution were compared. Fading of the recognition signal showed that the ricin molecules on the Au(111) surface interacted with aptamer molecules in the blocking solution instead of the one on the AFM tip.[27] We also conducted the blocking of recognition signal of ricin by injection of 1.3 μM antiricin antibody solution in PBS pH 7.2 into the flow-through liquid cell. In this antibody blocking experiment, the AFM tip was still modified by the aptamer. Therefore, the aptamer and

dx.doi.org/10.1021/jp301765n | J. Phys. Chem. B 2012, 116, 5316−5322

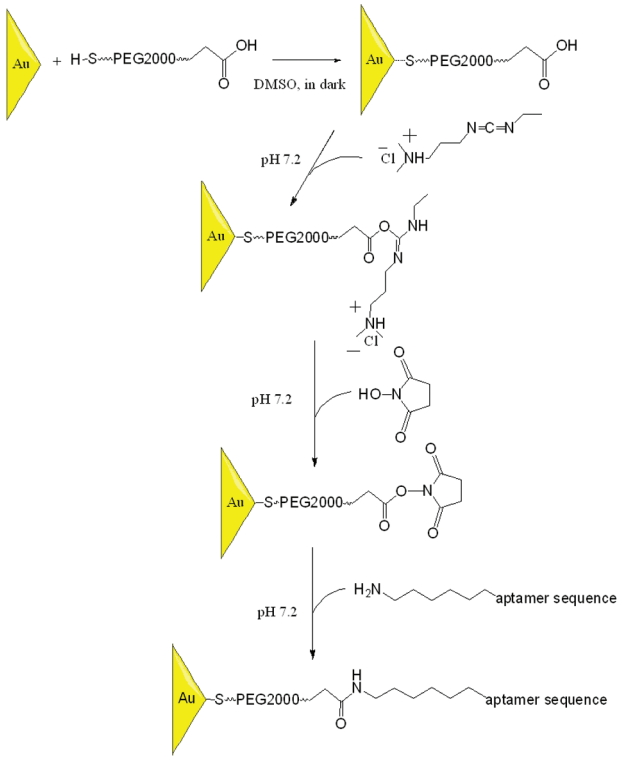

Figure 2. Reaction schemes used for AFM tip functionalization. Thiol group of the bifunctionalized PEG linker molecule formed a gold–sulfur bond with the gold film on the tip surface, and the carboxyl group at the other end of PEG reacted with the amine-modified aptamer to form the amide bond. Amine reaction was activated by EDC/NHS solution at pH 7.2.

antibody should not interfere with each other and should both be able to bind to ricin. AFM recognition images showed continuous recognition signals during the antibody blocking experiment, which proved that the antibody and aptamer have different binding sites. Details of the experimental results are given in the Results and Discussions.

The secondary structure of the antiricin aptamer (Figure 3a) was predicted by Mfold webserver.[33] The 3-dimensional folding structure of the aptamer was generated using nucleic acids builder (NAB), which is included in the Amber 10 molecular dynamics package.[34,35] The aptamer molecule was considered as an isobaric–isothermal ensemble (NTP), and the folding dynamics was conducted in the generalized Born (GB) implicit solvation model to predict a structure with the lowest energy (Figure 3a, cartoon representation). The entire simulation time for aptamer folding is 20 ps, and a longer simulation time did not change the folding structure. The ricin structure was obtained from PDB 2AAI (Figure 1).[36] The human IGG1 was modified according to the literature as a homological model to obtain the ricin–antibody complex structure (Figure 3b).[37,38]

Predictions of binding sites were based on the literature and conducted by molecular docking simulation (HADDOCK web server).[39,40] Binding conformations of ricin–aptamer and ricin–antibody complexes are shown in Figure 3. Docking results demonstrated that ricin has different binding sites for the aptamer and antibody, although they both locate on ricin A chain.[27] The molecular modeling method is also used to analyze the lysine–NHS ester reaction sites. The results (in the next section) show that the binding sites of ricin to aptamer and antibody were still available after immobilization. The

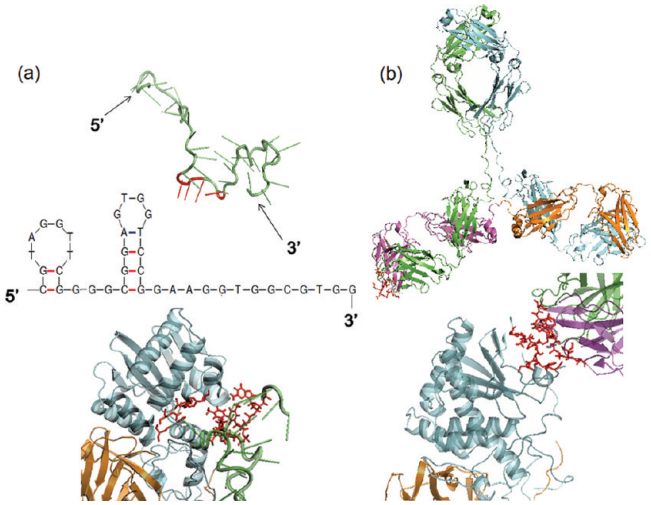

Figure 3. Simulated molecular structures of antiricin aptamer, antiricin antibody, and their binding conformations with ricin. Structures were predicted by molecular dynamics and molecular docking methods. (a) (Top) Aptamer secondary and tertiary structures. (Bottom) Ricin–aptamer binding conformation. Ricin A chain is in cyan. Binding residues of the ricin and aptamer are highlighted in red. (b) (Top) Structure of the antiricin antibody IGG1. (Bottom) Ricin–antibody binding conformation. Binding residues of the antibody and ricin are highlighted in red.

method of combining AFM experimental images and simulation structures is used in this paper to explain the different ricin conformations observed on the Au(111) surface and the high efficiency of molecular recognition. The results from AFM experiments and simulation are coherent with each other at the single-molecule level. However, we noticed that the predicted ricin–aptamer and ricin–antibody complexes were based on their structures without other constraints, such as chemical modifications, geometry and surface properties of the Au(111) substrate, and interference of the AFM tip. Therefore, simulation results only represent the most stable conformations of these molecules that freely exist in solutions, and their real conformations after chemical modifications on the gold surface may be different from the results shown here. Nevertheless, the simulation results and AFM measurements in this study agree well. Simulation of biomolecules on a certain surface/interface is a very interesting topic that is worth further investigation.

■ RESULTS AND DISCUSSION

In order to probe the aptamer–ricin and antibody–ricin interactions, we first immobilized ricin molecules on the Au(111) surface via one of ricin's nine lysine residues reacting with LA-NHS. To probe the details of interactions, it is important to know where the binding sites to aptamer or antibody locate on the ricin molecule surface. These locations of binding sites are determined by ricin conformations and orientations on the substrate. Inside the ricin molecule we established three axes to help locate the nine lysine residues, the predicted binding site to aptamer, and the predicted binding site to antibody (Figure 4a). These axes form right angles with each other in the 3 dimensions, approximately. The longest axis (z axis, red) is around 9 nm across the molecule, the second longest axis (x axis, black) is around 6 nm, and the shortest axis (y axis, purple) is around 5 nm, which are measured in molecular visualization software PyMOL (version 0.99rc6).[41] These axes are not used to showing strict

dx.doi.org/10.1021/jp301765n | J. Phys. Chem. B 2012, 116, 5316–5322

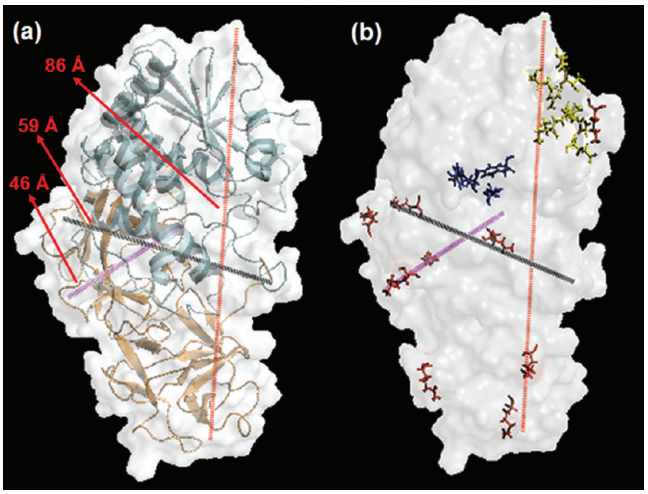

Figure 4. Three axes used to illustrate the locations of different active residues on ricin molecule. *x* axis (black), *y* axis (purple), and *z* axis (red) were established inside the ricin molecule. (a) Three axes and their relative positions to A chain (cyan) and B chain (orange). (b) Translucent surface representation of ricin structure and the three axes. Nine lysine residues are in red, predicted binding residues to aptamer are in blue, and predicted binding residues to antibody are in yellow.

coordination but to label the 3-dimentional orientation of the ricin molecule. All nine lysine residues were found to locate on the ricin surface and are highlighted in red. The binding sites to aptamer (blue) and antibody (yellow) both locate on the ricin A chain. The relative positions of all these reacting residues and binding sites to the three axes are shown in Figure 4b. We will use these three orientation axes as guiding lines to label ricin molecules and compare them with the ricin AFM images.

Figure 5 shows the representative AFM topography (Figure 5a) and recognition (Figure 5b) images. The average size of the

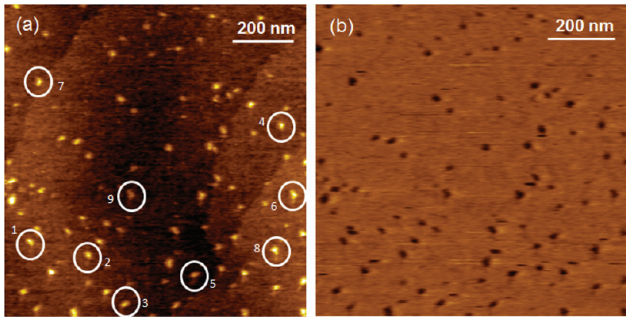

Figure 5. AFM topography image (a) and recognition image (b) of ricin molecules on Au (111) surface. Image size is 1000 nm × 1000 nm. Nine individual ricin molecules (1−9) were selected to represent different ricin conformations predicted by molecular modeling (see Figure 6).

ricin molecule in this figure is determined to be around 20 nm, which is consistent with a previous study using antibody.[16] The recognition image shows the corresponding recognition images of those ricin molecules, which demonstrated that the aptamer-modified AFM tip interacts with ricin molecules with a concentration as low as 20 pg/mL.

As shown in Figure 5, nine individual ricin molecules were highlighted and labeled 1−9 to represent the nine predicted conformations generated by NHS−lysine reaction. This reaction between NHS ester molecules and lysine residues on the protein surface has been widely used for immobilization and detection of proteins.[42] Lysine residues tend to locate on the outer surface of proteins because lysine is hydrophilic. This property of lysine plays an important role in protein tertiary structures in aqueous solutions and in turn influences the protein functions. Therefore, the different reacting lysine residues on the surface of an individual ricin molecule plays an important role on the ricin conformation on the gold substrate. The nine ricin molecules shown in Figure 5a correspond to nine probable binding conformations of ricin to the LA-NHS linker molecules on the Au (111) surface. The recognition image in Figure 5b shows that almost all ricin molecules in the topography image have the corresponding recognition image in Figure 5b. The recognition efficiency is 98% (100 out of 102), which is also similar to the high efficiency of recognition images generated by antibody.[16] These high efficiencies of recognition signals prove that the ricin A chains were able to directly expose their binding sites to aptamer and antibody in the bulk solution; otherwise, the aptamer or antibody on the AFM tips cannot approach the ricin binding sites during scanning. Although ricin can bind to NHS ester with different lysine residues and form different conformations and orientations on the Au(111) surface, the binding sites to the aptamers were available under most circumstances.

The detailed relationship between each ricin conformation and its LA-NHS reaction can be seen in Figure 6, which shows a comparison of zoom-in topography images and molecular modeling structures of ricin molecules on the Au(111) surface. The white dashed line crossing each ricin image represents the approximate position of the *z* axis inside the ricin molecule (explained in Figure 4). Simulation structures have been rotated to mimic both the top view and the side view of ricin molecules in the AFM topography images.

We classified the nine ricin conformations in Figure 5 into four groups since some of the topography images of the ricin molecules have very similar outlines. The simulation structures show that the similarity of the conformations in each group is based on the locations of the reacting lysine residues. In group I, conformations 1, 2, and 3 react with lysine B chain K168, K203, and K243, respectively. These lysine residues are close to each other on the ricin surface. In group II, the reacting residue is B chain K40 for conformation 4. In group III, the reacting residues of conformations 5 and 6 are B chain K52 and K62, respectively. These two lysine residues also locate very close to each other. In group IV, the reacting residues of conformations 7, 8, and 9 are B chain K219, A chain K4, and A chain K239, respectively. They are not close to each other, but their relative locations to the three axes are similar. Therefore, it is very difficult to distinguish their topography images among each other in the same group.

From Figure 6 we also found that most of the lysine residues on the ricin molecule are located in the ricin B chain, so the B chain is the most probably region bond to the NHS ester molecule on gold substrate. Therefore, the ricin A chain is supposed to contact with the bulk solution and in turn interact with either aptamer or antibody on the AFM tip.[16,27] For all conformations in groups I−III the ricin A chain is above the ricin B chain. For conformation IV, the A chain and B chain are at the same height level. Therefore, almost all of the ricin showed recognition signals in Figure 5b. For these conformations not showing recognition signals, the possible

dx.doi.org/10.1021/jp301765n | J. Phys. Chem. B 2012, 116, 5316−5322

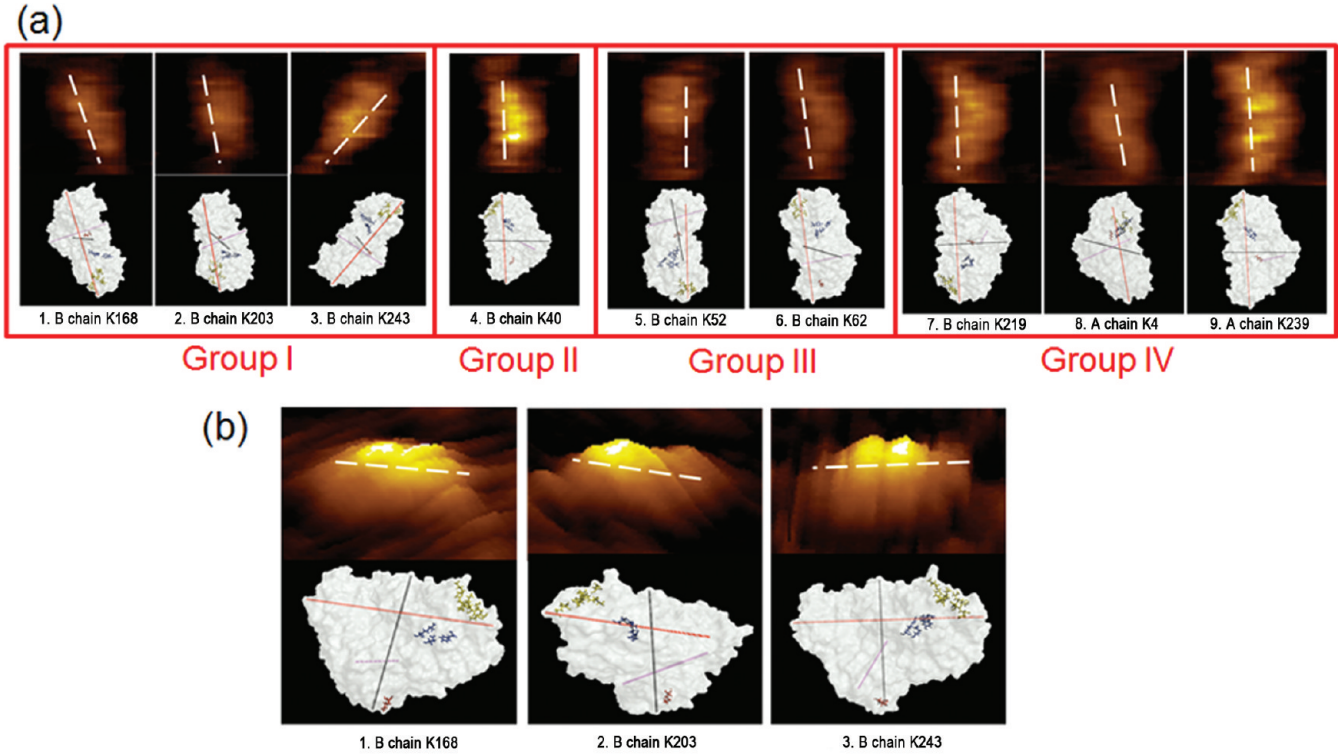

Figure 6. Zoom-in topography images of nine ricin conformations on Athe u(111) surface. Conformations 1−9 correspond with the ricin molecules 1−9 in Figure 5a. Image sizes are 40 nm × 40 nm for all conformations. (a) AFM topography images and predicted conformations shown in the top view. (b) 3-D topography images and predicted conformations of ricin 1, 2, and 3 shown in the side view.

reason could be that the binding between the aptamer on the AFM tip and the ricin on the substrate might be disturbed by the aqueous environment or the thermal noise.

To check the detailed structural information of these nine ricin conformations, we compared the 3D topography images of these nine conformations with the side view of the simulation structures. In Figure 6b the ricin simulation structures have been adjusted to show the predicted side view of each conformation above the gold substrate and LA-NHS layer. The 3D topography images show the relative positions of the ricin A chain and B chain along the AFM *z* axis (perpendicular to the substrate surface). The simulation structure of the same ricin conformation is put next to the 3D topography images, so that the predicted binding sites to aptamer and ricin can be seen in the comparison. When NHS ester bonds with ricin B chain K168 and K243, the ricin A chain and B chain were at approximately the same height level while the A chain was at a higher level than the B chain if ricin bonds with B chain K203. This minor change is very difficult to be distinguished in the 2D topography images.

To determine the distributions of the four conformations we also did statistical analysis on the ratio of these conformation groups (I−IV) and the recognition efficiency of these groups. The counting of different groups from four AFM topography images is shown in Figure 7. Detailed counting data is shown in SI-2, Supporting Information. The unknown group represents those images that cannot be distinguished or classified due to molecules overlapping, tip broadening, and compression effect.[43] If we neglect the group of "unknown", the most abundant conformations were from group I, which includes three conformations with the ricin B chain attached to LA-NHS. This trend is consistent with the proposed binding

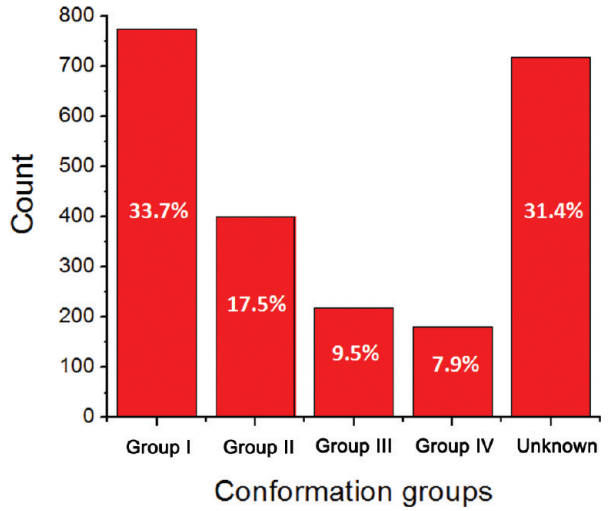

Figure 7. Distribution of different ricin conformations using NHS ester as a linker molecule. Ricin conformations determined by nine possible lysine reactions were classified into four groups (groups I−IV). "Unknown" group represents the remaining ricin conformations that cannot be distinguished and classified into any other groups. Abundances of groups I, II, III, and IV were 33.7%, 17.5%, 9.5%, and 7.9%, respectively. Relatively high abundance of the unknown group (31.4%) represents the experimental errors and limitations.

mechanism. The relatively large amount of conformations in the group "unknown" represents the limitation of the AFM technique we were using in the recognition experiments.[27] However, the overwhelming majority of the recognition of different ricin conformations shows the capability of the AFM

dx.doi.org/10.1021/jp301765n | J. Phys. Chem. B 2012, 116, 5316−5322

experiments and theoretical simulation approach in determining the molecular details of structures and interactions.

To determine the binding sites of aptamer and antibody to the ricin molecules we performed the interaction blocking as shown Figure 8. Figure 8a shows the results of the blocking experiment using aptamer solution. The recognition signal reduced significantly 46 min after injection of aptamer solution. The ricin binding sites to aptamer were blocked by other aptamers in the solution, so the aptamers on the AFM tip cannot bind to the ricin molecules and therefore cannot generate a recognition signal any more. Figure 8b shows the blocking experiment using antibody solution. The recognition image did not change for 40 min when using the aptamer-functionalized AFM tip. This result further proved that the aptamer and antibody bind to different sites on the ricin surface (as shown in Figure 3). Otherwise, the antibody in the solution will interfere with the binding site for the aptamer and reduce the recognition signal of ricin.

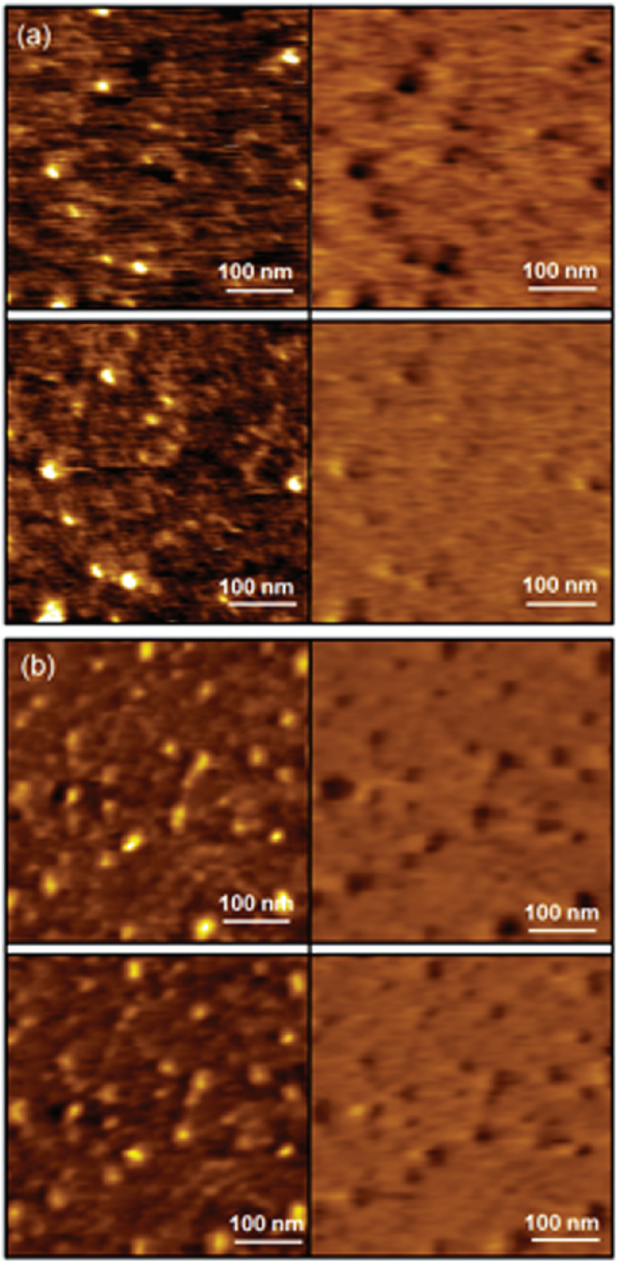

Figure 8. Blocking of the recognition signals generated by the aptamer-functionalized AFM tip. (a) Blocking of ricin recognition signals using 1 μM aptamer solution: (top) Before injection of aptamer and (bottom) 46 min after injection. Aptamer solution significantly reduced the recognition signals. (b) Blocking of ricin recognition signals using 1.3 μM antibody solution: (top) before injection of antibody and (bottom) 40 min after injection. Recognition signals did not fade away. Image size is 450 nm × 450 nm.

When comparing this experimental result with the molecular docking result, the AFM recognition experiments provide very helpful information on the binding sites of ricin to aptamer and antibody. Although we cannot distinguish the detailed binding residues and sequences using AFM, the recognition images and blocking test help us to confirm the availability of binding sites to aptamer and antibody on the ricin A chain after immobilization. Moreover, the difference of these two binding sites was verified by blocking experiments. This experimental result is also very useful for validation of simulation results, especially when another experimental method is not yet available to directly test the ricin−aptamer and ricin−antibody binding conformation.

CONCLUSIONS

We combined computational simulations and AFM recognition imaging to study the ricin conformations and its interactions with aptamer and antibody. The method used to immobilize ricin on the Au(111) surface makes it possible to obtain different ricin conformations due to specific covalent bonding between the LA-NHS ester and the lysine residues on the ricin surface. The ricin molecule conformations when reacting with different lysine residues were distinguished by AFM topography images. The simulated ricin structures confirmed that the different ricin conformations on the Au(111) surface were caused by different lysine residues reacting with the NHS ester. In addition, the ricin binding sites to aptamer and antibody were predicted by simulation methods and tested by blocking experiments. The binding sites for aptamer and antibody were not interfered by the immobilization method. This study demonstrated that the combination of experimental methods and molecular simulation methods could be used in binding studies of similar biospecies.

ASSOCIATED CONTENT

Supporting Information

Detailed description of the materials and reactions used for AFM tip modification; detailed results and discussion for statistical analysis of ricin conformations. This material is available free of charge via the Internet at http://pubs.acs.org.

AUTHOR INFORMATION

Corresponding Author

*Phone: 706-542-0502. Fax: 706-542-3804. E-mail: bxu@engr.uga.edu.

Notes

The authors declare no competing financial interest.

ACKNOWLEDGMENTS

We thank Drs. Robert Woods and Lachele Foley for guidance in modeling using AMBER software and Dr. Alexander Bonvin for his help on HADDOCK simulation. This research was supported in part by the National Science Foundation (ECCS 0823849, CBET 1139057).

REFERENCES

(1) Hermann, T.; Patel, D. J. *Science* **2000**, *287*, 820−825.
(2) Deniz, A. A.; Mukhopadhyay, S.; Lemke, E. A. *J. R. Soc. Interface* **2008**, *5*, 15−45.
(3) Musshoff, F.; Madea, B. *Drug Test. Anal.* **2009**, *1*, 184−191.
(4) Audi, J.; Belson, M.; Patel, M.; Schier, J.; Osterloh, J. *JAMA* **2005**, *294*, 2342−2351.
(5) Kim, Y.; Robertus, J. D. *Protein Eng.* **1992**, *8*, 775−779.
(6) Yan, X.; Day, P.; Hollis, T.; Monzingo, A. F.; Schelp, E.; Robertus, J. D.; Milne, G. W.; Wang, S. *Proteins* **1998**, *31*, 33−41.
(7) Hesselberth, J. R.; Miller, D.; Robertus, J.; Ellington, A. D. *J. Biol. Chem.* **2000**, *275*, 4937−4942.
(8) Tang, J.; Xie, J.; Shao, N.; Yan, Y. *Electrophoresis* **2006**, *27*, 1303−1311.
(9) Anderson, G. P.; Matney, R.; Liu, J. L.; Hayhurst, A.; Goldman, E. R. *BioTechniques* **2007**, *43*, 806−811.
(10) Fais, M.; Karamanska, R.; Allman, S.; Fairhurst, S. A.; Innocenti, P.; Fairbanks, A. J.; Donohoe, T. J.; Davis, B. G.; Russell, D. A.; Field, R. A. *Chem. Sci.* **2011**, *2*, 1952−1959.
(11) He, L.; Lamont, E.; Veeregowda, B.; Sreevatsan, S.; Haynes, C. L.; Diez-Gonzalez, F.; Labuza, T. P. *Chem. Sci.* **2011**, *2*, 1579−1582.
(12) Ding, S.; Gao, C.; Gu, L. *Anal. Chem.* **2009**, *81*, 6649−6655.
(13) Quan, C.; Liu, J. *Chinese J. Anal. Chem.* **2010**, *38*, 627−631.
(14) Pradhan, S.; Boopathi, M.; Kumar, O.; Baghel, A.; Pandey, P.; Mahato, T. H.; Singh, B.; Vijayaraghavan, R. *Biosens. Bioelectron.* **2009**, *25*, 592−598.
(15) Lin, L.; Wang, H.; Liu, Y.; Yan, H.; Lindsay, S. *Biophys. J.* **2006**, *90*, 4236−4238.
(16) Chen, G.; Ning, X.; Park, B.; Boons, G.; Xu, B. *Langmuir* **2009**, *25*, 2860−2864.
(17) Bizzarri, A. R.; Cannistraro, S. *Chem. Soc. Rev.* **2010**, *39*, 734−749.
(18) Yu, J.; Jiang, Y.; Ma, X.; Lin, Y.; Fang, X. *Chem. Asian J.* **2007**, *2*, 284−289.
(19) Lin, L.; Fu, Q.; Williams, B. A. R.; Azzaz, A. M.; Shogren-Knaak, M. A.; Chaput, J. C.; Lindsay, S. *Biophys. J.* **2009**, *97*, 1804−1807.
(20) Ellington, A. D.; Szostak, J. W. *Nature* **1990**, *346*, 818−822.
(21) Tuerk, C.; Gold, L. *Science* **1990**, *249*, 505−510.
(22) Forster, C.; Oberthuer, D.; Gao, J.; Eichert, A.; Quast, F. G.; Betzel, C.; Nitsche, A.; Erdmann, V. A.; Furste, J. P. *Acta Crystallogr., Sect. F: Struct. Biol. Cryst. Commun.* **2009**, *65*, 881−885.
(23) Nakamura, Y. *Adv. Polym. Sci.* **2011**, 1−18.
(24) Khati, M. *J. Clin. Pathol.* **2010**, *63*, 480−487.
(25) Radmacher, M.; Fritz, M.; Hansma, H. G.; Hansma, P. K. *Science* **1994**, *265*, 1577−1579.
(26) Hinterdorfer, P.; Baumgartner, W.; Gruber, H. J.; Schilcher, K.; Schindler, H. *Proc. Natl. Acad. Sci. U.S.A.* **1996**, *93*, 3477−3481.
(27) Wang, B.; Guo, C.; Chen, G.; Park, B.; Xu, B. *Chem. Commun.* **2012**, *48*, 1644−1646.
(28) Reyes, C. M.; Kollman, P. A. *J. Mol. Biol.* **2000**, *297*, 1145−1158.
(29) Pagano, B.; Martino, L.; Randazzo, A.; Giancola, C. *Biophys. J.* **2008**, *94*, 562−569.
(30) Saneyoshi, H.; Mazzini, S.; Avino, A.; Portella, G.; Gonzalez, C.; Orozco, M.; Marquez, V. E.; Eritja, R. *Nucleic Acid Res.* **2009**, 1−13.
(31) Hinterdorfer, P.; Kienberger, F.; Raab, A.; Gruber, H. J.; Baumgartner, W.; Kada, G.; Riener, C.; Wielert-Badt, S.; Borken, C.; Schindler, H. *Single Mol.* **2000**, *1*, 99−103.
(32) Chen, G.; Zhou, J.; Park, B.; Xu, B. *Appl. Phys. Lett.* **2009**, *95*, 043103.
(33) Zuker, M. *Nucleic Acid Res.* **2003**, *31*, 3406−3415.
(34) Case, D. A.; Darden, T. A.; Cheatham III, T. E.; Simmerling, C. L.; Wang, J.; Duke, R. E.; Luo, R.; Crowley, M.; Walker, R. C.; Zhang, W. et al. *AMBER 10*; University of California: San Francisco, 2008.
(35) Macke, T. J.; Case, D. A. In *Molecular Modeling of Nucleic Acids*; Leontes, N. B., SantaLucia, J. J., Eds.; American Chemical Society: Washington, D.C., 1998; pp 379−393.
(36) Rutenber, E.; Katzin, B. J.; Ernst, S.; Collins, E. J.; Mesna, D.; Ready, M. P.; Robertus, J. D. *Proteins* **1991**, *10*, 240−250.
(37) Padlan, E. A. *Mol. Immunol.* **1994**, *31*, 169−217.
(38) Neal, L. M.; O'Hara, J.; Brey, R. N., III; Mantis, N. J. *Infect. Immun.* **2010**, 552−561.
(39) Dijk, M. v.; Dijk, A. D. J. v.; Hsu, V.; Boelens, R.; Bonvin, M. J. J. *Nucleic Acid Res.* **2006**, *34*, 3317−3325.
(40) Vries, d. S. J.; Dijk, v. M.; Bonvin, A. M. J. J. *Nat. Protoc.* **2010**, *5*, 883−897.
(41) *The PyMOL Molecular Graphics System*, Version 1.2r3pre: Schrödinger, LLC: Portland, OR, 2010.
(42) Frasconi, M.; Mazzei, F.; Ferri, T. *Anal. Bioanal. Chem.* **2010**, *398*, 1545−1564.
(43) Raab, A.; Han, W. B., D.; Smith-Gill, S. J.; Lindsay, S. M.; Schindler, H.; Hinterdorfer, P. *Nat. Biotechnol.* **1999**, *17*, 901−905.